

Magnetic properties of highly ordered single crystals with layered YBaCuFeO₅ structure

Arnau Romaguera¹, Xiaodong Zhang¹, Ruyong Li¹, Oscar Fabelo² and José Luis García-Muñoz^{1*}

¹Institut de Ciència de Materials de Barcelona, ICMAB-CSIC, Campus UAB, 08193 Bellaterra, Spain

²Institut Laue-Langevin, 71 Avenue des Martyrs, 38042 Grenoble, France

Abstract. In the layered perovskites YBaCuFeO₅ (YBCFO) magnetic frustration stabilizes incommensurate spiral order up to unexpectedly high temperatures (T_S). The level of frustration and hence T_S depend directly on the fraction (n_d) of B-site (Cu/Fe) chemical disorder in the samples. We report a neutron investigation on the magnetic transitions in two YBaCuFeO₅ single crystals (one pure and the second slightly doped with Mn), grown by floating-zone methods, that present very low Fe/Cu cation disorder ($n_d \rightarrow 0$). The low density of antiferromagnetic Fe₂O₉ bipyramid units in these crystals precludes the stabilization of a frustrated topological network, which is at the origin of the non-collinear (helical) magnetic order. Instead, the ground state is substituted by two competing commensurate collinear magnetic phases, the majority one (\mathbf{k}_1) attributed to the perfectly ordered YBCFO perovskite ($n_d=0$). A second type of collinear magnetic domains (\mathbf{k}_2) develop for samples with disorder below a critical threshold ($0 < n_d < n_0$). Only in YBCFO samples with Cu/Fe disorder above the critical threshold a long-range helicoidal or spiral magnetic state can be formed.

1 Introduction

The materials presenting magnetic chirality form a rare class of frustrated compounds that attract a lot of attention owing to their unique technologically important properties. Among the properties realized in systems with chiral magnetic orders the multiferroicity is one of the most attractive. In frustrated magnets ordered spiral phases are particularly promising because the noncollinear spiral magnetic order breaks space-inversion symmetry and can induce spontaneous polarization through inverse Dzyaloshinsky-Moriya or spin-current mechanisms [1]. A common origin of polarization and spiral order guarantees a substantial coupling “by construction” in cycloidal multiferroic materials. Unfortunately, their low magnetic ordering temperatures (typically <50 K) critically restrict their potential use in spintronic and low-power magnetoelectric devices.

Exceptionally, the layered perovskites RBaCuFeO₅ have been reported to display spiral magnetic order (T_S) at unexpectedly high temperatures [2-6]. Surprisingly, there is no any apparent source of frustration in an ordered A- and B- site layered YBaCuFeO₅ structure. B-site metals form CuFeO₉ bilayers of corner-sharing Cu²⁺O₅ and Fe³⁺O₅ square pyramids that extend parallel to the ab plane. The bilayers formed by bipyramids are separated by Y³⁺ layers, and Ba²⁺ ions site within the bilayer spacing. Samples are prepared with partial Fe/Cu order in the structure, and the absence of perfect B-site cation order is at the origin of magnetic frustration [3-6]. In addition YBCFO exhibits an extraordinary

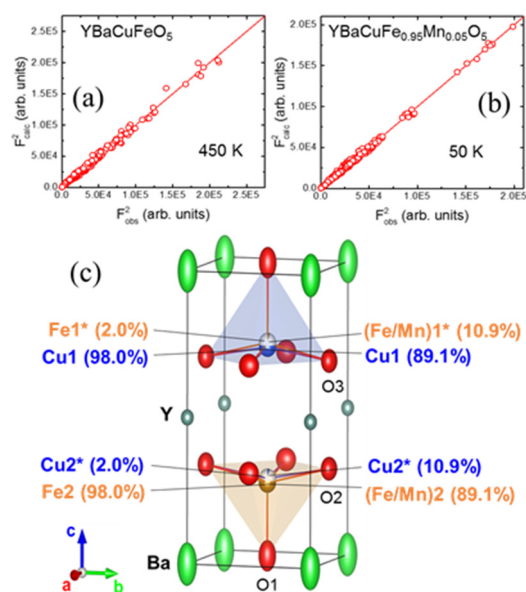


Fig. 1. Agreement plots of the nuclear structure refinements (calculated structure factors plotted against the integrated SCND nuclear reflections collected in D9@ILL) on the two single crystals of composition (a) YBaCuFeO₅ (450 K) and (b) YBaCuFe_{0.95}Mn_{0.05}O₅ (50 K). (c) Scheme of the refined $P4mm$ unit cell of the YBCFO crystal showing the refined amount of Fe/Cu disorder. The color of each pyramid corresponds to that of the dominant cation in it (blue: Cu; brown: Fe).

* Corresponding author: garcia.munoz@icmab.es

tunability of its spiral ordering temperature [4,5] ($T_S=T_{N2}$), which can be increased by 180 K (up to ~ 366 K [5]), by increasing the Cu/Fe chemical disorder in the bipyramids.

A collinear commensurate ($\mathbf{k}_1=[1/2, 1/2, 1/2]$) antiferromagnetic (AF) phase below $T_{N1} = 440$ K is followed by an incommensurate (ICM, $\mathbf{k}_2=[1/2, 1/2, 1/2\pm q]$) spiral magnetic order ($T_S=T_{N2} \sim 230$ K). Coinciding with the incommensurate magnetic order, the reported electrical polarization (P) reached $0.4 \mu\text{C}/\text{cm}^2$ in some polycrystalline specimens [2,3].

The need to extend these studies to single crystals led us to grow YBaCuFeO₅ crystals by floating zone. In this work the magnetic properties of two different crystals of compositions YBaCuFeO₅ and YBaCuFe_{0.95}Mn_{0.05}O₅ are here reported. Remarkable differences are found when comparing the crystals with their polycrystalline counterparts. Typically, B-site disorder in single crystals and powder samples is very different, and confirm the relevance of Cu/Fe disorder for the properties of these layered perovskites. This study has allowed extending the investigation on this layered structure to the regime of low Fe/Cu disorder.

2 Experimental

Single crystalline samples were grown in our Crystal Growth Lab. at the ICMAB by a modified traveling solvent floating zone (TSFZ) method from previously sintered polycrystalline rods of YBaCuFeO₅ and YBaCuFe_{0.95}Mn_{0.05}O₅. Hereafter named as YBCFO and YBCFO-5%Mn, respectively. The powders to make the rods were previously prepared as described in refs. [5,9]. A solvent consisting of CuO with 2 wt% B₂O₃ was used for the crystal growth of these incongruently melting compositions [7]. Further details on the growing conditions can be found in refs. [8,9]. In the ingot the c-axis of the YBCFO structure was perpendicular to the FZ growth direction (parallel to (110)). The elemental composition of the crystals was assessed by Inductively Coupled Plasma Optical Emission Spectroscopy (ICP-OES) that confirmed no deviations from the nominal molar ratios. Their quality and orientation was characterized by neutron Laue images and their stoichiometry, including the oxygen content, was further confirmed by single crystal neutron diffraction.

Neutron diffraction experiments on both crystals were performed at the high-flux reactor of the Institut Laue Langevin (ILL, Grenoble, France). Three different single-crystal instruments were used: Orient Express (to prove the crystal orientation), CYCLOPS (Laue single-crystal diffractometer) and D9 (hot-neutrons four-circle diffractometer, using $\lambda=0.837$ Å). The program RACER was used to integrate the omega- and omega-2theta-scans and to correct them for the Lorentz factor [11]. Data reduction and neutron refinements were made using the Fullprof package of programs [12]. Additionally the two-axis D20 diffractometer was also used ($\lambda=2.41$ Å) to characterized a powdered sample.

Table 1. Crystal structure of the single crystals and agreement factors obtained from the refinement of the D9@ILL single crystal neutron intensities ($\lambda=0.837$ Å). (*: minority fraction; n_d (disorder=Occ (Fe1*/Cu2*)). The coordinates of each metal (M: Cu or Fe) are constrained by $z(M1)+z(M2)=1$).

<i>P4mm</i>		YBaCuFeO ₅ (450 K)	YBaCuFe _{0.95} Mn _{0.05} O ₅ (50 K)
<i>a</i> = <i>b</i> (Å)		3.8815 (6)	3.8699 (3)
<i>c</i> (Å)		7.6839 (1)	7.6359 (3)
<i>z</i> (Y)	1 <i>a</i> (00 <i>z</i>)	0.4979 (3)	0.4979 (3)
<i>z</i> (Ba)	1 <i>a</i> (00 <i>z</i>)	0	0
<i>z</i> (Cu1)	1 <i>b</i> (½ ½ <i>z</i>)	0.7221 (3)	0.7326 (8)
<i>z</i> (Fe2)	1 <i>b</i> (½ ½ <i>z</i>)	0.2570 (3)	0.2657 (8)
<i>z</i> (Fe1*)	1 <i>b</i> (½ ½ <i>z</i>)	0.7430 (3)	0.7343 (8)
<i>z</i> (Cu2*)	1 <i>b</i> (½ ½ <i>z</i>)	0.2779 (3)	0.2674 (8)
<i>z</i> (O1)	1 <i>b</i> (½ ½ <i>z</i>)	0.0019 (8)	-0.002 (5)
<i>z</i> (O2)	1 <i>b</i> (½ 0 <i>z</i>)	0.3149 (6)	0.312 (4)
<i>z</i> (O3)	1 <i>b</i> (½ 0 <i>z</i>)	0.6814 (7)	0.682 (4)
Chemical order			
$n_d = \text{Occ (Fe1*/Cu2*)}$		0.020 (22)	0.109 (26)
1- $n_d = \text{Occ (Cu1/Fe2)}$		0.980 (22)	0.891 (26)
χ^2		2.27	1.12
R_F		7.83	2.95
R_F^2		8.32	4.36

3 Results

3.1 Structural characterization and Fe/Cu disorder

The structure of the two single domain crystals was studied using hot-neutrons ($\lambda=0.836$ Å) at the D9 four-circle neutron diffractometer. From data collected in D9 we determined the atomic positions in the non-centrosymmetric *P4mm* structure and partial Cu/Fe occupancies in the two pyramids of the unit cell. Extinction corrections were applied following the Becker-Coppens model. Fig. 1 displays the observed and calculated squared structure factors for the nuclear structure of the two crystals, refined from 537 nuclear reflections (295 independent). Among the structural information shown in Table 1 for both crystals, the degree of Fe/Cu cationic disorder (n_d) is crucial for the properties of this system. The magnetic *3d* metals (M) occupy the two pyramids of the unit cell [sites 1*b* (1/2 1/2 *z*) with $z \approx 0.74$ and $z \approx 0.27$ for, respectively, the upper and the lower pyramids in the Fig.1)]. The *z*-coordinates of the two positions that a given metal M (either Fe or Cu) can occupy in the cell (M1 and M2) were constrained in the form $z(M1)+z(M2)=1$. The upper (lower) pyramid in Fig. 1c is mainly occupied by Cu1 (Fe2). Therefore, the improper occupancy associated to the positions Fe1* and Cu2* is a measure of the disorder. The most important observation is the low level of Fe/Cu cation disorder (n_d) in the crystals: $n_d=0.020(22)$ and $0.109(26)$ for YBCFO and YBCFO-5%Mn, respectively. It should be noted that the cationic disorder found in powder samples is always much higher (above 30 %). So, the very low disorder in our

single crystals (which is also disclosed in Fig. 1c) need to be compared with $n_d \approx 0.32$, the typical cationic disorder found in powder samples cooled at 300°C/h after the last annealing [5]. A first central finding is, hence, that the complex TSFZ technique used to fabricate the crystals clearly favors the ordering of B-site cations. On one hand, this entails a serious drawback to dispose of disordered crystals with cycloidal order at ambient conditions. On the other hand, the study of these crystals allows us to explore highly ordered zones of the T - n_d phase diagram that are very difficult to access with samples prepared by ceramic methods in polycrystalline form. As an example, the lowest disorder reported in Ref. [5] in powder samples was $n_d \approx 0.29(3)$ applying a very slow controlled cooling rate of 10 °C/h.

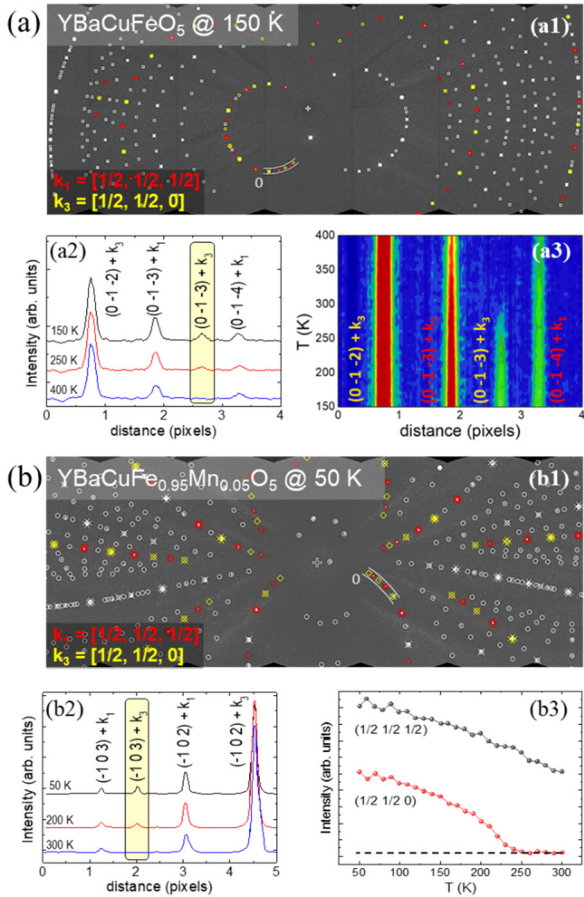


Fig. 2. Sections of the neutron Laue images collected at CYCLOPS@ILL at low temperature on the two single crystals, showing the indexation of nuclear reflections (in white) and the magnetic ones with $k_1=(1/2,1/2,1/2)$ and $k_3=(1/2,1/2,0)$ (in red and yellow, respectively; some magnetic reflections have also nuclear contribution). (a1) YBaCuFeO_5 (150 K) and (b1) $\text{YBaCuFe}_{0.95}\text{Mn}_{0.05}\text{O}_5$ (50 K). Panels (a2) and (b2) show a comparison of the integrated profiles along selected regions of the area detectors at three characteristic temperatures. The evolution with temperature of the magnetic phases is depicted in (a3) as a 2D contour map of the integrated Laue profiles, and in (b3) by the evolution of the integrated intensity of $(1/2,1/2,1/2)$ and $(1/2,1/2,0)$ reflections collected in D9@ILL.

1.2 Magnetic characterization by single-crystal neutron diffraction

With regards to the magnetic properties, the central observation is the lack of incommensurate spiral order in the crystals. Fig. 2 shows the temperature dependent magnetic information obtained on the neutron Laue diffractometer CYCLOPS (ILL), from measurements in the range 50-400 K. As shown in the indexed Laue patterns (Figs. 2a1 and 2b1) the magnetic phases present in the crystals are all commensurate. The antiferromagnetic phases with propagation vectors $k_1=(1/2, 1/2, 1/2)$ (AF1) and $k_3=(1/2, 1/2, 0)$ (AF3) are found to coexist at low temperatures in both crystals. Warming the crystals from the base temperature, the evolution of the integrated profiles for some selected characteristic magnetic reflections are displayed in Figs. 2a (YBCFO) and 2b (YBCFO-5%Mn). From the observed intensities, the collinear AF1 order is in both crystals the majority magnetic phase and the AF3 order is the minority one. Furthermore we observed that, under heating, the former (AF1) is always more stable than the AF3 configuration. The respective transition temperatures are $T_{N1}=435$ K and $T_{N3}=290$ K for YBCFO, and $T_{N1}=420$ K and $T_{N3}=242$ K for YBCFO-5%Mn.

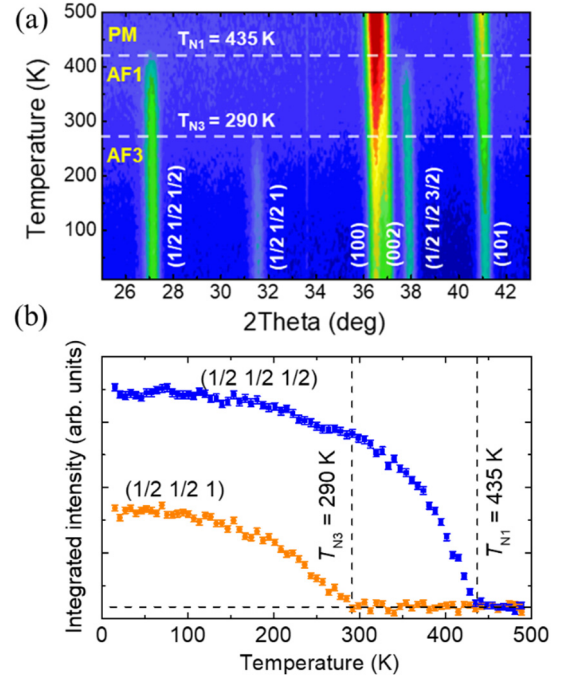


Fig. 3. Evolution of magnetic order in a powdered sample of the highly ordered YBCFO single-crystal from neutron diffraction (D20@ILL). (a) Contour map showing the 2θ - T projection of the temperature dependence for the NPD intensities at the low Q -range. (b) Thermal evolution of the integrated intensities of the $(1/2,1/2,1/2)$ and $(1/2,1/2,1)$ magnetic reflections associated to the AF1 (k_1) and AF3 (k_3) phases, respectively.

Additionally, in YBCFO we also performed neutron powder diffraction (NPD) measurements on a powdered sample that we obtained by crushing a portion of our large ingot. We used D20 to collect NPD patterns ($\lambda=2.41 \text{ \AA}$) within the temperature range 10 to 500 K. The evolution in this interval of the main magnetic reflections in YBCFO obtained by NPD measurements is illustrated in Figs. 3a,b. The neutron Rietveld refinement at 10 K for the powdered YBCFO sample is exposed in Fig. 4a.

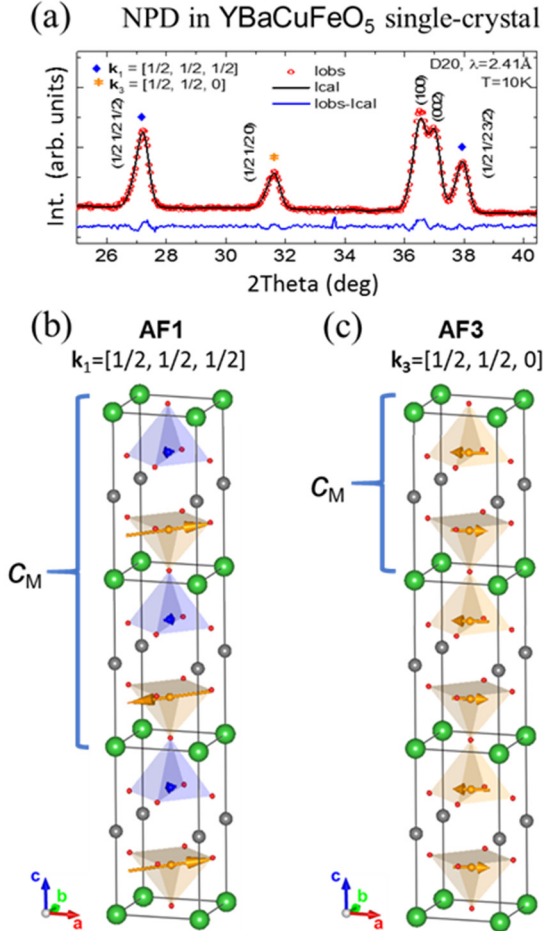


Fig. 4. (a) Rietveld refinement (black curve) of the D20@ILL ($\lambda=2.41 \text{ \AA}$) neutron diffraction pattern (red circles) at 10 K for the powdered YBCFO single crystal with very high Fe/Cu order (blue diamonds and orange stars indicate AF1 and AF3 magnetic reflections, respectively). Projections of the refined collinear magnetic orders with propagation vectors (b) $k_1=(1/2,1/2,1/2)$ and (c) $k_3=(1/2,1/2,0)$. The different periodicity along- c is illustrated with the help of the c_M parameter for each magnetic unit cell. For the sake of clarity, only the majoritarian magnetic atom (M) is shown in the pyramids (blue: Cu; brown: Fe)

In the T - n_d phase diagram showed in Fig. 5 the magnetic transition temperatures are plotted as a function of Cu/Fe disorder (n_d). In this phase diagram we have gathered the information from our two highly ordered crystals and the magnetic phase transitions reported in Ref. [5] for a set of more disordered YBCFO polycrystalline samples with increasing cationic disorder that were originally prepared in powder form

by applying different cooling rates. To be highlighted is the existence of three different regimes in the YBaCuFeO₅ phase diagram versus disorder and the fact that the non-collinear (spiral) order does not form if the level of Fe/Cu disorder in the structure is too high (beyond the triple point) or too low (below a critical threshold, n_0).

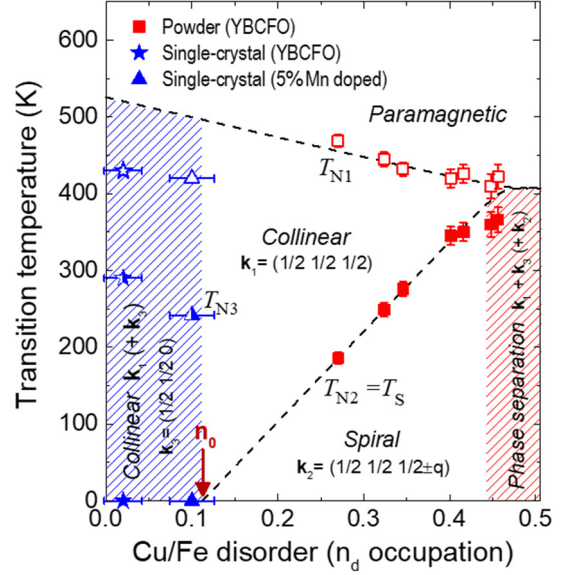


Fig. 5. Magnetic phase diagram versus Fe/Cu cation disorder for YBCFO. Dashed lines describe the phase boundaries from the onset of the magnetic phases according to neutron diffraction data, obtained on YBCFO powder samples (red squares, from Ref. [5]). The n_d - T values from the two highly ordered single crystals described in this work are also shown (blue symbols). The two crystals fall within the $0 < n_d < n_0$ region, below the critical threshold of disorder for developing spiral magnetic order in this structure. Empty and filled points correspond to T_{N1} and $T_{N2}=T_S$, respectively, and the half-filled ones correspond to T_{N3} .

Fig. 5 reveals that the two crystals investigated in this work fall into the first phase separated region (low disorder), and consequently must be regarded as representative of the system when $n_d < n_0$. The dashed lines in Fig. 5 are lineal fits to the experimental points. A direct comparison between the ordering temperatures in the two crystals is difficult due to their slightly different composition. However the magnetic evolutions depicted in Figs. 2 and 3 for both samples strongly suggest that the AF1 and AF3 collinear magnetic phases appear in distinct regions of the crystal. The AF3 regions only order more than 100 K below the formation of AF1 magnetic domains. But the magnetic regions with $k_3=(1/2, 1/2, 0)$ do not substitute to the AF1 phase but rather coexists with it. It is of interest to note that, as shown in Fig. 4c, the coupling between the two spins inside the bipyramids is antiferromagnetic in the AF3 regions. In contrast to the AF1 domains, where the magnetic atoms in FeCuO₉ bipyramids exhibit the expected ferromagnetic coupling dictated by the positive sign of the Fe^{3+} -O-Cu²⁺ exchange (see Fig. 4b). Therefore, the second type of domains (with collinear AF3 order and $k_3=(1/2, 1/2, 0)$ propagation vector) are

very likely associated to zones in the crystal with higher cationic disorder where the Fe-Cu ferromagnetic coupling inside the bipyramids has been substituted by antiferromagnetic Fe₂O₉ and Cu₂O₉ bipyramids. From our refinement of the NPD pattern for YBCFO shown in Fig. 4a equal average ordered moments were found in the AF3 bipyramids ((~43%) $m(M1) \approx m(M2) \approx 1.12(5) \mu_B$ at 10 K, parallel to *ab* plane). In the AF1 phase (~57%) we found $m(M2) = 2.65(3) \mu_B$ antiferromagnetically coupled to $m(M1) = 0.32(4) \mu_B$, these moments separated 11(7)° from the *ab* plane ($\chi^2 = 4.6$, $R_B = 1.6$, $R_M(AF1) = 4.3$, $R_M(AF3) = 5.1$).

4 Conclusions

In the layered perovskites with YBCFO structure the level of magnetic frustration and hence T_S depend directly on the fraction n_d of Cu/Fe cation disorder in the samples. Two single crystalline samples have been grown by TSFZ methods that present very low levels of Fe/Cu disorder: $n_d = 0.020(22)$ and $0.109(26)$. Their study by neutron diffraction has allowed extending our comprehension of the magnetic properties of these systems to the low-disorder range.

From the study of the two crystals several relevant conclusions can be drawn. First, the lack of (noncollinear) helicoidal or spiral order in these layered perovskites with low cationic disorder at the B-site. Second, although the study gives support to the “*order by disorder*” theoretical framework in this system [13,14], it also reveals that there is a critical threshold of disorder (n_0), below which a long-range spiral magnetic state cannot be formed. In this structure the critical threshold must be greater than ~10(3)%, the disorder (n_d) in our less ordered crystal. Fig. 5 confirms that this conclusion (at odd with some previous assumptions in this system) is in agreement with the linear extrapolation of the experimental (n_d, T_S) points (filled red points in Fig. 5) corresponding to YBCFO powder samples reported earlier in ref. [5]. Dashed lines in Fig. 5 are simply guides to the eye. Third, a phase separated or inhomogeneous region emerges in the phase diagram when disorder is too low. Below the threshold n_0 an insufficient density of strongly antiferromagnetic Fe₂O₉ bipyramids (named “impurity bonds” in Ref. [13] and having a central role for generating frustration) cannot stabilize long-ranged non-collinear domains (spiral order). Nevertheless in the small fraction of non-mixed M₂O₉ bipyramid units (M₂=Fe₂ or Cu₂) the M-O-M exchange is antiferromagnetic and this favors the emergence of magnetic domains with wave vector $\mathbf{k}_3 = (1/2, 1/2, 0)$ inside the AF1 matrix (\mathbf{k}_1) dominated by ferromagnetic FeCuO₉ bipyramids.

Due to the difficulties preparing powder YBCFO samples with a very high Fe/Cu cationic order, the high-order region of the phase diagram was until now almost unexplored. The tendency in single crystals to adopt highly ordered configurations allows overcome such limitations.

Acknowledgments.- Financial support from the Ministerio de Ciencia, Innovación y Universidades (MINCIU), Projects No. PID2021-124734OB-C22 and RTI2018-098537-B-C21, cofunded by ERDF from EU, and “Severo Ochoa” Programme for Centres of Excellence in R&D [FUNFUTURE (CEX2019-000917-S)]. R.L.’s work was done as a part of the Ph.D program in Materials Science at Universitat Autònoma de Barcelona. We also acknowledge the Institut Laue-Langevin (ILL) for provision of beam time (Easy-445 and Easy-447, Test-2882 and dois:10.5291/ILL-DATA.5-14-273, 10.5291/ILL-DATA.5-14-277 and 10.5291/ILL-DATA.5-31-2680 5-41-1153).

References

1. I. A. Sergienko and E. Dagotto, Phys. Rev. B **73**, 094434 (2006)
2. B. Kundys, A. Maignan, and C. Simon, Appl. Phys. Lett. **94**, 072506 (2009)
3. M. Morin *et al.*, Phys. Rev. B **91**, 064408 (2015)
4. M. Morin, E. Canévet, A. Raynaud, M. Bartkowiak, D. Sheptyakov, V. Ban, M. Kenzelmann, E. Pomjakushina, K. Conder, and M. Medarde, Nat. Commun. **7**, 13758 (2016)
5. A. Romaguera, X. Zhang, O. Fabelo, F. Fauth, J. Blasco and J. L. García-Muñoz, Phys. Rev. Research **4**, 043188 (2022)
6. T. Shang, E. Canévet, M. Morin, D. Sheptyakov, M. Teresa Fernández-Díaz, E. Pomjakushina, M. Medarde, M. T. Fernández-Díaz, E. Pomjakushina, and M. Medarde, Sci. Adv. **4**, eaau6386 (2018)
7. Y.C. Lai *et al.*, J. Phys. Condens. Matter **29**, 145801 (2017)
8. A. Romaguera Camps, PhD Thesis. Universitat Autònoma de Barcelona. 2023
9. X. Zhang, A. Romaguera, F. Sandiumenge, O. Fabelo, J. Blasco, J. Herrero-Martín, and J. L. García-Muñoz, J. Magn. Magn. Mater. **551**, 169165 (2022).
10. X. Zhang, A. Romaguera, O. Fabelo, F. Fauth, J. Herrero-Martín, and J. L. García-Muñoz, Acta Mater. **206**, 116608 (2021)
11. M. S. Lehmann, Acta Cryst. A. **30**, 580 (1974)
12. J. Rodríguez-Carvajal, Phys. B Phys. Condens. Matter **192**, 55 (1993)
13. A. Scaramucci, H. Shinaoka, M. V. Mostovoy, M. Müller, C. Mudry, M. Troyer, and N. A. Spaldin, Phys. Rev. X **8**, 011005 (2018).
14. A. Scaramucci, H. Shinaoka, M. V. Mostovoy, R. Lin, C. Mudry, and M. Müller, Phys. Rev. Res. **2**, 013273 (2020).